Preprint accepted for publication in Journal of Computational Physics, 2013

http://dx.doi.org/10.1016/j.jcp.2013.09.024

First, Second, and Third Order Finite-Volume Schemes for Diffusion

Hiroaki Nishikawa *
National Institute of Aerospace, Hampton, VA 23666

October 10, 2013

Abstract

In this paper, we present constructions of first, second, and third order schemes for diffusion by the method introduced in [J. Comput. Phys., 227 (2007) 315-352]. In this method, numerical schemes for diffusion are constructed by advection schemes via an equivalent hyperbolic system. This paper demonstrates that the method enables straightforward constructions of diffusion schemes for finite-volume methods on unstructured grids. In particular, it is demonstrated that a robust first-order upwind scheme leads to a robust first-order diffusion scheme, and a high-order advection scheme leads to a high-order diffusion scheme. It is shown that first, second, and third order schemes are capable of producing first, second, and third order accurate solution gradients, respectively, on irregular grids. Accuracy, Fourier stability, and the energy stability of the developed schemes are discussed. A new hyperbolic diffusion system having virtually no source terms is also introduced to simplify the construction of the third-order scheme. Numerical results are presented for regular and irregular triangular grids to demonstrate not only the superior accuracy but also the accelerated steady convergence over a traditional method.

1 Introduction

Ever-increasing computing speed and parallelism are allowing the use of high-fidelity computational fluid dynamics (CFD) models in engineering analysis and design involving complex flow fields. However, the current state-of-the-art for unstructured CFD codes still need improvements in efficiency and accuracy required for engineering design and optimization, especially for turbulent flow simulations on unstructured grids [1, 2]. In particular, the derivative quantities needed to evaluate the design such as viscous/heat fluxes and vorticity are obtained with a lower order accuracy on unstructured grids, e.g., fully adapted viscous grids. Also, current state-of-the-art Naver-Stokes codes are known to produce erratic viscous stress and heating distributions for hypersonic viscous simulations even on a regular grid [3, 4, 5]. Resolution of these problems is very important for justifying the use of high-fidelity models in aerodynamic design and optimization. Progress has been made towards overcoming these problems by improved inviscid methods [6, 7], but a general capability of producing high-accuracy in these derivative quantities on general irregular grids has yet to be in place. Such a capability is highly desirable for efficient viscous simulations over complex geometries with grid adaptation. Furthermore, practical finite-volume CFD codes often rely on robust but inconsistent viscous discretizations such as the edge-terms-only scheme [8] or a positivity-enforced Galerkin scheme for the sake of robustness. The use of inconsistent schemes can provide some degree of robustness, but it can lead not only to wrong solutions [9] but also to convergence deterioration [8]. There is a critical need for developing a robust and consistent scheme for diffusion on general unstructured grids.

We tackle these problems by a radical method introduced in Ref.[10]. In this method, the steady state solution to the diffusion equation is computed by integrating in time an equivalent first-order hyperbolic system to the steady state. This method has been shown to offer a number of advantages

*National Institute of Aerospace, 100 Exploration Way, Hampton, VA 23666-6147, USA. Tel.:+1 757 864 7244. *E-mail address:* hiro@nianet.org

over conventional methods, including drastic simplifications in discretization (i.e., advection scheme for diffusion), orders of magnitude acceleration in steady convergence by explicit schemes, and the equal order of accuracy for the solution and the gradients (viscous/heat fluxes). These advantages have been demonstrated for the diffusion equation[10] and the advection-diffusion equation[11] by the second-order residual-distribution method, and later for the compressible Navier-Stokes equations [12], which were made hyperbolic with the viscous/heat fluxes added as extra variables, by the second-order finite-volume method. Simply because the diffusion equation is converted to a first-order hyperbolic system, virtually all existing methodologies for hyperbolic systems are directly applicable to diffusion. It is now possible, therefore, that a robust first-order advection scheme generates a robust first-order diffusion scheme, and a high-order advection scheme generates a high-order diffusion scheme.

In this paper, we focus on finite-volume schemes for diffusion. We demonstrate that the method enables straightforward constructions of diffusion schemes including first and third order schemes, which are highly valuable components for robust and accurate viscous discretizations on unstructured grids. We discuss the energy estimate of the hyperbolic diffusion system, and show that the upwind flux leads to an energy-stable first-order scheme for diffusion. For second and third order schemes, we consider two types of constructions. One is a straightforward finite-volume construction, and the other takes advantage of the extra variables carried in the hyperbolic system to avoid gradient computation for the solution variable. It is shown that the latter yields more economical schemes and these schemes produce significantly more accurate solutions than those generated by the former. Third-order schemes are constructed by the third-order finite-volume scheme of Katz and Sankaran developed for hyperbolic systems[13], which is thus directly applicable to the hyperbolic system for diffusion. To simplify the construction of the third-order schemes, we introduce a fully hyperbolic diffusion system having no source terms. Numerical results are presented for both regular and irregular triangular grids. Developed schemes are compared with a representative traditional scheme. It is demonstrated that first, second, and third order diffusion schemes are capable of producing the solution and the gradients to the same order of accuracy on both regular and irregular triangular grids with orders-of-magnitude accelerations in steady convergence.

2 Hyperbolic Diffusion System

Consider the diffusion equation in two dimensions:

$$\partial_t u = \nu \left(\partial_{xx} u + \partial_{yy} u\right), \tag{1}$$

where ν is a constant diffusion coefficient. Following Ref. [10], we consider computing the steady state solution to the diffusion equation (1) by solving the following first-order hyperbolic diffusion system:

$$\begin{aligned} \partial_t u &= \nu \left(\partial_x p + \partial_y q\right), \\ \partial_t p &= \left(\partial_x u - p\right)/T_r, \\ \partial_t q &= \left(\partial_y u - q\right)/T_r, \end{aligned} \tag{2}$$

where p and q are the gradient variables, which relax to the solution derivatives, $\partial_x u$ and $\partial_y u$, respectively, in the steady state, and T_r is a *free parameter* called the relaxation time. Note that the system is equivalent to the diffusion equation (1) in the steady state for arbitrary T_r, and thus, inherently, the system is not stiff in contrast to the hyperbolic heat equation of Cattaneo[14]. Write the system in the vector form,

$$\partial_t \mathbf{U} + \partial_x \mathbf{F} + \partial_y \mathbf{G} = \mathbf{S}, \tag{3}$$

where

$$\mathbf{U} = \begin{bmatrix} u \\ p \\ q \end{bmatrix}, \quad \mathbf{F} = \begin{bmatrix} -\nu p \\ -u/T_r \\ 0 \end{bmatrix}, \quad \mathbf{G} = \begin{bmatrix} -\nu q \\ 0 \\ -u/T_r \end{bmatrix}, \quad \mathbf{S} = \begin{bmatrix} 0 \\ -p/T_r \\ -q/T_r \end{bmatrix}. \tag{4}$$

Consider the flux Jacobian of the flux projected along an arbitrary vector, $\mathbf{n} = (n_x, n_y)$:

$$\mathbf{A}_n = \frac{\partial(\mathbf{H}\cdot\mathbf{n})}{\partial \mathbf{U}} = \frac{\partial(\mathbf{F}n_x + \mathbf{G}n_y)}{\partial \mathbf{U}} = \begin{bmatrix} 0 & -\nu n_x & -\nu n_y \\ -n_x/T_r & 0 & 0 \\ -n_y/T_r & 0 & 0 \end{bmatrix}, \tag{5}$$

where $\mathbf{H} = [\mathbf{F}, \mathbf{G}]$ is the flux tensor. It has the following eigenvalues:

$$\lambda_1 = -\sqrt{\frac{\nu}{T_r}}, \quad \lambda_2 = \sqrt{\frac{\nu}{T_r}}, \quad \lambda_3 = 0. \tag{6}$$

The eigenvalues are independent of $\mathbf{n}$, and therefore the system describes a wave propagating isotropically. The third eigenvalue corresponds to the inconsistency damping mode[10], acting on the components of p and q such that $q_x - p_y \neq 0$. The relaxation time T_r does not affect the steady solution, and thus can be defined solely for the purpose of accelerating the convergence to the steady state[10, 11]. Following Ref. [10], we define T_r as

$$T_r = \frac{L_r^2}{\nu}, \quad L_r = \frac{1}{2\pi}, \tag{7}$$

where the length scale, L_r, has been defined to maximize the effect of propagation as will be discussed later. The relaxation time thus defined is large enough to destroy the equivalence between the diffusion equation and the hyperbolic system during the time evolution towards the steady state. The hyperbolic system here designed specifically for steady computations is simply called the hyperbolic diffusion system. Time-accurate computation is possible by implicit time integration schemes, e.g., utilizing the dual-time stepping method [15, 16], but it is beyond the scope of the present paper. The absolute Jacobian, $|\mathbf{A}_n|$ is constructed by the right-eigenvector matrix, $\mathbf{R}_n$, and the diagonal eigenvalue-matrix, $\mathbf{\Lambda}_n$,

$$\mathbf{R}_n = \frac{1}{2}\begin{bmatrix} 1 & -1 & 0 \\ n_x/L_r & n_x/L_r & -2n_y \\ n_y/L_r & n_y/L_r & 2n_x \end{bmatrix}, \quad \mathbf{\Lambda}_n = \begin{bmatrix} -\lambda & 0 & 0 \\ 0 & \lambda & 0 \\ 0 & 0 & 0 \end{bmatrix}, \tag{8}$$

where $\lambda \equiv |\lambda_1| = |\lambda_2| = \sqrt{\nu/T_r} = \nu/L_r$, as follows:

$$|\mathbf{A}_n| = \mathbf{R}_n|\mathbf{\Lambda}_n|\mathbf{R}_n^{-1} = \lambda \begin{bmatrix} 1 & 0 & 0 \\ 0 & n_x^2 & n_x n_y \\ 0 & n_x n_y & n_y^2 \end{bmatrix}. \tag{9}$$

The hyperbolicity implies that the system has a characteristic form. Multiplying the hyperbolic diffusion system by $\mathbf{R}_n^{-1}$ from the left decouples the system into three characteristic equations in the direction $\mathbf{n}$:

$$\partial_t w_1 - \lambda\, \partial_n w_1 = -\lambda\, p_n, \quad \partial_t w_2 + \lambda\, \partial_n w_2 = -\lambda\, p_n, \quad \partial_t w_3 = -\frac{w_3}{T_r}, \tag{10}$$

where

$$\partial_n = n_x\partial_x + n_y\partial_y, \quad p_n = pn_x + qn_y, \quad w_1 = L_r p_n + u, \quad w_2 = L_r p_n - u, \quad w_3 = qn_x - pn_y. \tag{11}$$

It shows that the first two characteristic variables, w_1 and w_2, are propagated at the same speed in the negative and positive directions, respectively, and they are also damped by the source term whereas the third variable w_3 is purely damped (inconsistency damping mode).

3 Energy Estimate

We define the energy associated with the hyperbolic diffusion system as

$$E \equiv \frac{u^2 + L_r^2(p^2 + q^2)}{2}. \tag{12}$$

The governing equation for the energy can be derived by multiplying the hyperbolic system (3) by the row vector, $\boldsymbol{\ell}^E = (u, L_r^2 p, L_r^2 q)$, from the left:

$$\partial_t E + \partial_x f^E + \partial_y g^E = -\nu(p^2 + q^2), \tag{13}$$

where

$$f^E = -\nu u p, \quad g^E = -\nu u q. \tag{14}$$

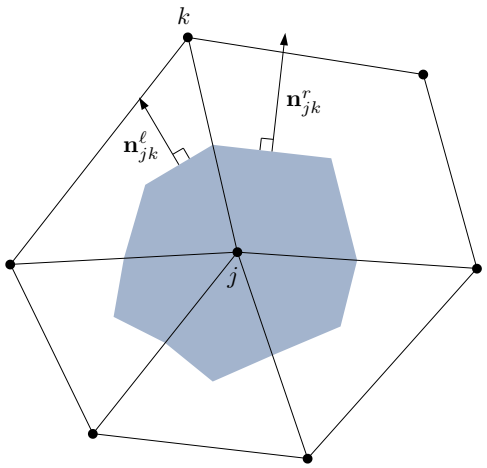

Figure 1: Dual control volume for the node-centered finite-volume method with scaled outward normals associated with an edge, $\{j, k\}$.

By integrating the energy equation over the domain Ω, we obtain

$$\frac{d}{dt}\int_\Omega E\,dV = -\oint_{\partial\Omega} \mathbf{f}^E \cdot \mathbf{n}\,dA - \nu\int_\Omega (p^2+q^2)\,dV, \tag{15}$$

where $\partial\Omega$ denotes the boundary of the domain, $\mathbf{f}^E = (f^E, g^E)$, $\mathbf{n}$ is the unit outward normal vector, and dA denotes the infinitesimal boundary area. This integral form shows that the total energy is damped by the magnitude of the solution gradient and changed only by the boundary flux. In the steady state, we have $(p, q) = \nabla u = (\partial_x u, \partial_y u)$, and the energy estimate reduces to

$$\int_\Omega \nabla u \cdot \nabla u\,dV - \oint_{\partial\Omega} u\frac{\partial u}{\partial n}dA = 0, \tag{16}$$

which is the well-known energy estimate of the Laplace equation. It is a manifestation of the fact that the hyperbolic diffusion system is equivalent to the diffusion equation in the steady state.

4 Node-Centered Edge-Based Finite-Volume Schemes

4.1 Discretization

The node-centered edge-based finite-volume scheme for Equation (3) is given by

$$V_j\frac{d\mathbf{U}_j}{dt} = -\sum_{k\in\{k_j\}} \Phi_{jk}A_{jk} + \mathbf{S}_j V_j, \tag{17}$$

where V_j is the dual volume, $\{k_j\}$ is a set of neighbors of the node j, Φ_{jk} is a numerical flux, and A_{jk} is the magnitude of the directed area vector, i.e., $A_{jk} = |\mathbf{n}_{jk}| = |\mathbf{n}^\ell_{jk} + \mathbf{n}^r_{jk}|$ (see Figure 1). This formulation is valid for general unstructured grids. Note also that an appropriate boundary flux must be supplied at the boundary node. For example, the simplest boundary flux would be the one point quadrature:

$$V_j\frac{d\mathbf{U}_j}{dt} = -\sum_{k\in\{k_j\}} \Phi_{jk}A_{jk} + \mathbf{S}_j V_j - \sum_{j\in\{j_b\}} \mathbf{H}_j \cdot \hat{\mathbf{n}}^b_j A^b_j, \tag{18}$$

where $\{j_b\}$ is a set of boundary nodes, and $\hat{\mathbf{n}}^b_j$ and A^b_j are, respectively, the unit outward normal vector and the magnitude of the boundary portion of the dual volume around a boundary node $j \in \{j_b\}$. For first-order schemes, it is sufficiently accurate, but for second-order schemes, a different quadrature is required for the linear exactness in the flux integration. See Ref.[9] for a comprehensive list of linearity preserving boundary quadrature formulas. We evaluate the numerical flux by the upwind flux:

$$\Phi_{jk} = \frac{1}{2}(\mathbf{H}_L + \mathbf{H}_R)\cdot\hat{\mathbf{n}}_{jk} - \frac{1}{2}|\mathbf{A}_n|(\mathbf{U}_R - \mathbf{U}_L), \tag{19}$$

where $\hat{\mathbf{n}}_{jk}$ is the unit directed area vector, and $\mathbf{A}_n$ is defined as the normal flux Jacobian along $\hat{\mathbf{n}}_{jk}$,

$$\mathbf{A}_n = \frac{\partial(\mathbf{H}\cdot\hat{\mathbf{n}}_{jk})}{\partial\mathbf{U}}. \tag{20}$$

The left and right states are obtained by the nodal solutions for first-order accuracy and by the linear extrapolation from the nodes for second/third-order accuracy as we will discuss later. We numerically integrate the semi-discrete system (17) towards the steady state to obtain the steady solution, which will be the steady solution to the diffusion equation (1). The global time step is defined as the minimum of the local time steps defined by

$$\Delta t_j = \mathrm{CFL}\frac{2V_j}{\sum\limits_{k\in\{k_j\}}(\nu/L_r A_{jk} + V_j/T_r)}. \tag{21}$$

The maximum CFL number depends on the scheme construction as well as the time-integration scheme, and will be determined later. It should be noted here that the time step is $O(h)$ and that it is significantly larger than a typical diffusion time step of $O(h^2)$. It leads to $O(1/h)$ acceleration in the steady convergence over traditional methods. This ever-increasing acceleration factor has been shown to bring a tremendous acceleration in steady computations for the diffusion, the advection-diffusion, and the compressible Navier-Stokes equations [10, 11, 12].

4.2 First-Order Scheme

For first-order accuracy, we evaluate the left and right states by the nodal solutions:

$$\mathbf{U}_L = \mathbf{U}_j, \qquad \mathbf{U}_R = \mathbf{U}_k. \tag{22}$$

The upwind flux is then given by

$$\Phi_{jk} = \frac{1}{2}(\mathbf{H}_j + \mathbf{H}_k)\cdot\hat{\mathbf{n}}_{jk} - \frac{1}{2}|\mathbf{A}_n|(\mathbf{U}_k - \mathbf{U}_j). \tag{23}$$

This completes the construction of the first-order diffusion scheme. To investigate the energy stability, we multiply the semi-discrete equation (17) by the vector $\boldsymbol{\ell}_j^E$ from the left to get

$$V_j\frac{dE_j}{dt} = -\sum_{k\in\{k_j\}}\boldsymbol{\ell}_j^E\Phi_{jk}A_{jk} - \nu(p_j^2+q_j^2)V_j, \tag{24}$$

which is summed over a set of nodes, $\{j\}$, to give

$$\sum_{j\in\{j\}}V_j\frac{dE_j}{dt} = \sum_{e\in\{e\}}(\boldsymbol{\ell}_k^E - \boldsymbol{\ell}_j^E)\Phi_{jk}A_{jk} - \sum_{j\in\{j\}}\nu(p_j^2+q_j^2)V_j - \sum_{j\in\{j_b\}}\boldsymbol{\ell}_j^E\mathbf{H}_j\cdot\hat{\mathbf{n}}_j^b A_j^b, \tag{25}$$

where $\{e\}$ is a set of edges, and the relation $\Phi_{jk} = -\Phi_{kj}$ has been used to obtain the first term. Note also that the last term is the boundary flux contribution from the semi-discrete equation (18) defined at boundary nodes. It can be expanded as follows:

$$\sum_{j\in\{j\}}V_j\frac{dE_j}{dt} = \sum_{e\in\{e\}}(\mathbf{f}_k^E - \mathbf{f}_j^E)\cdot\hat{\mathbf{n}}_{jk}A_{jk} - 2\sum_{j\in\{j_b\}}\mathbf{f}_j^E\cdot\hat{\mathbf{n}}_j^b A_j^b - \sum_{j\in\{j\}}\nu(p_j^2+q_j^2)V_j - \frac{\nu}{2L_r}\sum_{e\in\{e\}}\epsilon_{jk}A_{jk}, \tag{26}$$

where

$$\epsilon_{jk} = (u_k-u_j)^2 + L_r^2\left[(p_k-p_j, q_k-q_j)\cdot\hat{\mathbf{n}}_{jk}\right]^2 \geq 0. \tag{27}$$

Note that the last term on the right hand side, which is the contribution from the dissipation term, is nonpositive, and it is $O(h)$ smaller than others. It is easy to show by converting the first term as a sum over the nodes that the first term on the right hand side cancel out except on the boundary; the remaining contribution cancels the half of the boundary flux sum. We thus finally obtain the discrete energy estimate for the first-order scheme:

$$\sum_{j\in\{j\}}V_j\frac{dE_j}{dt} = -\sum_{j\in\{j_b\}}\mathbf{f}_j^E\cdot\hat{\mathbf{n}}_j^b A_j^b - \sum_{j\in\{j\}}\nu(p_j^2+q_j^2)V_j - \frac{\nu}{2L_r}\sum_{e\in\{e\}}\epsilon_{jk}A_{jk}, \tag{28}$$

which can be written also by arranging the boundary contribution in the form of the trapezoidal rule over each boundary edge as

$$\sum_{j\in\{j\}} V_j \frac{dE_j}{dt} = -\sum_{e\in\{e_b\}} \frac{\mathbf{f}_1^E + \mathbf{f}_2^E}{2} \cdot \hat{\mathbf{n}}_e^b A_e^b - \sum_{j\in\{j\}} \nu(p_j^2 + q_j^2) V_j - \frac{\nu}{2L_r} \sum_{e\in\{e\}} \epsilon_{jk} A_{jk}, \tag{29}$$

where $\{e_b\}$ is a set of boundary edges, the subscripts 1 and 2 denote the end nodes of an edge $e \in \{e_b\}$, $\hat{\mathbf{n}}_e^b$ and A_e^b are, respectively, the unit outward normal and the magnitude of the edge. For the central scheme (zero dissipation), it is a discrete analog of the energy estimate (15). For the upwind scheme, the dissipation acts as reducing the energy, and thus the energy cannot increase by the dissipation. That is, the central scheme is energy consistent, and the upwind scheme is energy stable. It is a valid conclusion for triangular, quadrilateral, and mixed grids. Moreover, the energy-stable first-order upwind scheme for diffusion is applicable to cell-centered finite volume methods also.

It is worth pointing out that the central flux yields a scheme of different nature: the discrete equations are decoupled and the gradient variables are explicitly computed from the solution values by the edge-based Green-Gauss method. The scheme, then, reduces to a traditional scheme: second-order accurate for the solution and first order accurate for the gradidents on irregular grids. Moreover, the explicit time step will be $O(h^2)$, not $O(h)$ any more. It is known that the central scheme applied to the hyperbolic diffusion system leads, in the same way, to the Bassi-Rebay scheme in the discontinuous Galerkin method. See Ref.[9] for details. In this paper, we will not discuss the central scheme any further.

To derive an optimal length scale, L_r, we consider the first-order scheme on a regular quadrilateral grid for the sake of simplicity. Consider the Fourier mode, $\mathbf{U}_0 \exp i(\beta_x x/h + \beta_y y/h)$, which is defined on a regular grid of uniform spacing h. $\mathbf{U}_0$ is a vector of amplitudes. β_x and β_y are the frequencies in x and y directions, respectively, and $i = \sqrt{-1}$. We insert the Fourier mode into the semi-discrete scheme and obtain the evolution equation for $\mathbf{U}_0$ in the form:

$$\frac{d\mathbf{U}_0}{dt} = \mathbf{M}\mathbf{U}_0, \tag{30}$$

where the matrix is found for smooth components to be

$$\mathbf{M} = \begin{bmatrix} -\dfrac{\nu\beta^2}{2hL_r} & \dfrac{i\nu\beta_x}{h} & \dfrac{i\nu\beta_y}{h} \\ \dfrac{i\nu\beta_x}{hL_r^2} & -\dfrac{\nu}{L_r^2} & 0 \\ \dfrac{i\nu\beta_y}{hL_r^2} & 0 & -\dfrac{\nu}{L_r^2} \end{bmatrix}, \tag{31}$$

where $\beta^2 = \beta_x^2 + \beta_y^2$. The eigenvalues are given by

$$-\frac{\nu}{L_r^2}, \quad -\frac{\nu}{2L_r^2}\left(1 + \frac{\beta^2}{2h} \pm \sqrt{1 - \frac{L_r\beta^2}{h} + \frac{L_r^2\beta^2}{4h^2}(\beta^2 - 16)}\right). \tag{32}$$

Following Ref.[10], we define L_r such that the last two eigenvalues to be complex conjugate to maximize the effect of error propagation. By setting the expression inside the square root to be nonpositive for all frequencies, we obtain

$$L_r \le \frac{2}{\pi(\pi h + 4)}. \tag{33}$$

In this paper, for the sake of simplicity, we take

$$L_r = \frac{1}{2\pi}, \tag{34}$$

for all schemes.

4.3 Second-Order Schemes

4.3.1 Scheme I

For second-order accuracy, we compute the nodal gradients by a linear least-squares method, and evaluate the left and right states by the linear extrapolation from the nodes:

$$\mathbf{U}_L = \mathbf{U}_j + \frac{1}{2}\nabla\mathbf{U}_j \cdot \Delta\mathbf{l}_{jk}, \qquad \mathbf{U}_R = \mathbf{U}_k - \frac{1}{2}\nabla\mathbf{U}_k \cdot \Delta\mathbf{l}_{jk}, \tag{35}$$

where $\Delta\mathbf{l}_{jk} = (x_k - x_j, y_k - y_j)$, and $\nabla\mathbf{U}_j$ and $\nabla\mathbf{U}_k$ are the solution gradients computed by the least-squares method at j and k, respectively. The numerical flux is computed by the upwind flux (19). The discrete energy estimate differs from the first-order scheme by the contribution from the nodal gradients:

$$\sum_{j\in\{j\}} V_j \frac{dE_j}{dt} = -\sum_{j\in\{j_b\}} \mathbf{f}_j^E \cdot \hat{\mathbf{n}}_j^b A_j^b - \sum_{j\in\{j\}} \nu(p_j^2 + q_j^2)V_j - \frac{\nu}{2L_r}\sum_{e\in\{e\}} \epsilon_{jk}A_{jk} - \frac{\nu}{2L_r}\sum_{e\in\{e\}} \gamma_{jk}A_{jk}, \tag{36}$$

where the term involving the nodal gradients is indicated by γ_{jk},

$$\gamma_{jk} = \Delta w_1 \widetilde{\Delta w}_{1j} + \Delta w_2 \widetilde{\Delta w}_{2k}. \tag{37}$$

Here, the following notations have been introduced:

$$\Delta w_1 = w_{1k} - w_{1j}, \quad \Delta w_2 = w_{2k} - w_{2j}, \quad \widetilde{\Delta w}_{1j} = \nabla w_{1j} \cdot \Delta\mathbf{l}_{jk}, \quad \widetilde{\Delta w}_{2j} = \nabla w_{2j} \cdot \Delta\mathbf{l}_{jk}. \tag{38}$$

The energy stability depends on the sign of γ_{jk}. The scheme is strictly energy-stable if $\gamma_{jk} \geq 0$, e.g., if the edge-projection of the nodal gradients of the characteristic variables shares the sign with the corresponding edge-derivative along the edge. Note that the last two terms on the right hand side are $O(h)$ smaller than the first two consistent terms. It is also noted that we can always ensure the energy stability by ignoring the gradients, i.e., by reverting back to the energy-stable first-order scheme. The above discrete energy equation corresponds to the point integration of the boundary flux, which is linearity-preserving for quadrilateral elements. If the linearity-preserving boundary quadrature for triangles [9] is used, then we obtain

$$\sum_{j\in\{j\}} V_j \frac{dE_j}{dt} = -\sum_{e\in\{e_b\}} \overline{\mathbf{f}^E} \cdot \hat{\mathbf{n}}_e^b A_e^b - \sum_{j\in\{j\}} \nu(p_j^2 + q_j^2)V_j - \frac{\nu}{2L_r}\sum_{e\in\{e\}} \epsilon_{jk}A_{jk} - \frac{\nu}{2L_r}\sum_{e\in\{e\}} \gamma_{jk}A_{jk}, \tag{39}$$

where $\overline{\mathbf{f}^E}$ is defined, with $\mathbf{f}^E(u,p,q) = (-\nu up, -\nu uq)$, as

$$\overline{\mathbf{f}^E} = \frac{3\mathbf{f}^E(u_1,p_1,q_1) + 2\mathbf{f}^E(u_1,p_2,q_2) + 2\mathbf{f}^E(u_2,p_1,q_1) + 3\mathbf{f}^E(u_2,p_2,q_2)}{10}. \tag{40}$$

The resulting boundary quadrature is still exact for linear fluxes over each boundary edge.

On a regular triangular grid as shown in Figure 3(a), we substitute smooth functions into the scheme and expand it to get

$$\frac{du_j}{dt} = \nu(\partial_x p + \partial_y q) - \frac{\nu h^2}{12}\left[\partial_{xx}(\partial_x p + \partial_y q) + \partial_{xy}(\partial_x p + \partial_y q) + \partial_{yy}(\partial_x p + \partial_y q)\right] + O(h^3), \tag{41}$$

$$\frac{dp_j}{dt} = \frac{1}{T_r}(\partial_x u - p) - \frac{h^2}{12T_r}\left[\partial_{xxx}u + \partial_{xyy}u + \partial_{xxy}u\right] + O(h^3), \tag{42}$$

$$\frac{dq_j}{dt} = \frac{1}{T_r}(\partial_y u - q) - \frac{h^2}{12T_r}\left[\partial_{yyy}u + \partial_{xyy}u + \partial_{xxy}u\right] + O(h^3). \tag{43}$$

Note that the gradients are defined by the central-difference in the analysis, and therefore they are second-order accurate. If the smooth functions are the exact steady solutions, then we obtain the truncation error, (τ_u, τ_p, τ_q):

$$\tau_u = O(h^3), \tag{44}$$

$$\tau_p = -\frac{h^2}{12T_r}\partial_{xxy}u + O(h^3), \tag{45}$$

$$\tau_q = -\frac{h^2}{12T_r}\partial_{xyy}u + O(h^3). \tag{46}$$

The truncation error in the first equation is $O(h^3)$. This is a special property of the edge-based finite-volume scheme on triangles with second-order gradients[13]. On the other hand, the truncation errors in other equations are $O(h^2)$ because the point integration of the source term is not compatible with the edge-based flux integration scheme to third-order accuracy. Therefore, the scheme is second-order accurate even with second-order gradients. It is second-order accurate for both solution and gradient variables.

Note that the above analysis is presented just for the sake of comparison and by no means intended to be a rigorous mathematical proof of accuracy. Such a proof is not necessary because the reconstruction-based edge-based finite-volume scheme has been well studied and already known to be second-order accurate on arbitrary triangular grids for hyperbolic systems [17]. The same applies to all truncation error analyses presented in the rest of the paper, including those for third-order schemes that are also known to be third order accurate on arbitrary triangular grids for hyperbolic systems.

4.3.2 Scheme II

The second-order upwind diffusion scheme constructed in the previous section produces accurate solution gradients, (p_j, q_j). We may then replace the least-squares gradients of the main variable by (p_j, q_j):

$$u_L = u_j + \frac{1}{2}(p_j, q_j) \cdot \Delta\mathbf{l}_{jk}, \qquad u_R = u_k - \frac{1}{2}(p_k, q_k) \cdot \Delta\mathbf{l}_{jk}, \tag{47}$$

This scheme, called Scheme II, is more economical than Scheme I because gradient computations are not necessary for the main variable. Gradient computations are required only for the gradient variables. The energy estimate is essentially the same as that of Scheme I, but with the following changes:

$$\nabla u_j = (p_j, q_j), \quad \nabla u_k = (p_k, q_k), \tag{48}$$

in the computation of ∇w_{1j} and ∇w_{2k} for γ_{jk}. Again, the construction of an energy-stable second-order scheme is beyond the scope of the present paper.

For Scheme II, the Taylor expansion provides insights not only on the accuracy but also on the stability in the time integration. On a regular triangular grid in Figure 3(a), we substitute smooth functions into the scheme and expand it to get

$$\begin{aligned}
\frac{du_j}{dt} &= \nu(\partial_x p + \partial_y q) \\
&- \frac{\nu h}{6L_r}\left[(\sqrt{2}+\sqrt{5})\partial_x(p-\partial_x u) + \sqrt{2}\partial_y(p-\partial_x u) + \sqrt{2}\partial_x(q-\partial_y u) + (\sqrt{2}+\sqrt{5})\partial_y(q-\partial_y u)\right] \\
&- \frac{\nu h^2}{12}\left[\partial_{xx}(\partial_x p + \partial_y q) + \partial_{xy}(\partial_x p + \partial_y q) + \partial_{yy}(\partial_x p + \partial_y q)\right] + O(h^3), \\
\frac{dp_j}{dt} &= \frac{1}{T_r}(\partial_x u - p) - \frac{h^2}{6T_r}\left[\partial_{xx}(p-\partial_x u) + \partial_{xy}(p-\partial_x u) + \partial_{xy}(q-\partial_y u) + \frac{1}{2}(\partial_{xx}p + \partial_{yy}p + \partial_{xx}q)\right] + O(h^3), \\
\frac{dq_j}{dt} &= \frac{1}{T_r}(\partial_y u - q) - \frac{h^2}{6T_r}\left[\partial_{yy}(q-\partial_y u) + \partial_{xy}(q-\partial_y u) + \partial_{xy}(p-\partial_x u) + \frac{1}{2}(\partial_{xx}q + \partial_{yy}q + \partial_{xx}p)\right] + O(h^3).
\end{aligned}$$

Suppose that the smooth functions are the numerical solutions. Then, the above equations show how the numerical solutions evolve in time. Noting that the first equation has a first-order spatial error term, we expect that Scheme II will be stable with the forward Euler time-integration, which is not true for typical second-order schemes. Suppose, on the other hand, that the smooth functions are the exact steady solutions. Then, we obtain the truncation error, (τ_u, τ_p, τ_q):

$$\tau_u = O(h^3), \tag{49}$$

$$\tau_p = -\frac{h^2}{12T_r}(\partial_{xx}p + \partial_{yy}p + \partial_{xx}q) + O(h^3), \tag{50}$$

$$\tau_q = -\frac{h^2}{12T_r}(\partial_{xx}q + \partial_{yy}q + \partial_{xx}p) + O(h^3). \tag{51}$$

Again, the truncation error in the first equation is $O(h^3)$ because of the second-order accurate gradients, but not in other equations for the same reason mentioned in the previous section. In order to achieve third-order accuracy, it is necessary to discretize the source term in a compatible manner, which is the subject of the next section.

4.4 Third-Order Schemes

We construct third-order diffusion schemes following the work of Katz and Sankaran[13]. The third-order scheme of Katz and Sankaran was introduced for the Euler equations and it is generally applicable to hyperbolic systems. Therefore, it is directly applicable to the hyperbolic diffusion system. They demonstrated that the node-centered edge-based finite-volume scheme can achieve third-order accuracy on triangular grids if the nodal gradients are computed to second-order accuracy and the flux is linearly extrapolated to the edge-midpoint in the case of nonlinear equations. The third-order accuracy has been demonstrated for regular as well as irregular triangular grids in Refs. [13, 18, 19]. In applying the third-order scheme to our hyperbolic diffusion system, we need to discretize the source term carefully. The need for a careful discretization for source terms has been as pointed out in Ref. [13] and described in the form of a matching truncation error problem in Ref.[20]. It is known that the point integration as we have done in the first and second order schemes will not work. Currently, two general techniques are available for achieving third-order accuracy for equations with a source term. One is to discretize the source term by an extended Galerkin discretization formula[21]. Another is to write the source term in the divergence form as suggested in Ref.[20], so that it can be discretized straightforwardly by the third-order scheme. However, both techniques typically require computations of the second derivatives of the source term. To avoid computations of the second derivatives, we introduce a special divergence form for the hyperbolic diffusion system.

4.4.1 Fully Hyperbolic Diffusion System

We propose to express the source term in the hyperbolic diffusion system in the divergence form:

$$\mathbf{S} \to \partial_x \mathbf{F}^s + \partial_y \mathbf{G}^s, \tag{52}$$

so that the whole system can be written as

$$\partial_t \mathbf{U} + \partial_x \tilde{\mathbf{F}} + \partial_y \tilde{\mathbf{G}} = 0, \tag{53}$$

where $\tilde{\mathbf{F}} = \mathbf{F} - \mathbf{F}^s$, $\tilde{\mathbf{G}} = \mathbf{G} - \mathbf{G}^s$, and

$$\mathbf{F}^s = \begin{bmatrix} 0 \\ (y - y_j)\, q/T_r \\ -(x - x_j)\, q/T_r \end{bmatrix}, \quad \mathbf{G}^s = \begin{bmatrix} 0 \\ -(y - y_j)\, p/T_r \\ (x - x_j)\, p/T_r \end{bmatrix}, \tag{54}$$

where (x_j, y_j) denotes the coordinates of a node j in a computational grid. That is, the system is defined locally around each node in the grid. It is straightforward to derive the governing equation for $\omega = q_x - p_y$, which is a consistency constraint on p and q, from the last two equations:

$$\partial_t \omega + \left(\frac{x - x_j}{T_r}\right) \partial_x \omega + \left(\frac{y - y_j}{T_r}\right) \partial_y \omega = -\frac{3\omega}{T_r}, \tag{55}$$

which shows that ω is convected and damped. The convective behavior implies the third wave that now propagates at a finite speed:

$$\lambda_3 = \frac{(x - x_j)n_x + (y - y_j)n_y}{T_r}. \tag{56}$$

For this reason, we call the modified system (53) the fully hyperbolic diffusion system. The fully hyperbolic diffusion system is equivalent to the following:

$$\begin{aligned} \partial_t u &= \nu\,(\partial_x p + \partial_y q), \\ T_r \partial_t p &= (\partial_x u - p) + (y - y_j)\,\omega, \\ T_r \partial_t q &= (\partial_y u - q) - (x - x_j)\,\omega. \end{aligned} \tag{57}$$

The terms proportional to ω on the right hand side vanish precisely at the node j. Therefore, the fully hyperbolic system is consistent with the original system at the node j. These extra terms appear to introduce $O(h)$ errors in the neighborhood of j, but ω vanishes in the steady state and thus they do not affect the accuracy of the scheme as will be shown later by truncation error analysis. Also, it has

no effect on the energy estimate (15). We emphasize that the fully hyperbolic formulation is built upon the constraint, $\omega = 0$. The technique can be extended to other types of equations and source terms provided such constraints exist and can be incorporated into the divergence formulation of source terms.

Note that the fully hyperbolic diffusion system is not unique. For example, we may define the source term fluxes also as

$$\mathbf{F}^s = \begin{bmatrix} 0 \\ -(x-x_j)\,p/T_r \\ -(y-y_j)\,p/T_r \end{bmatrix}, \quad \mathbf{G}^s = \begin{bmatrix} 0 \\ -(x-x_j)\,q/T_r \\ -(y-y_j)\,q/T_r \end{bmatrix}, \tag{58}$$

which lead to

$$\begin{aligned} \partial_t u &= \nu\,(\partial_x p + \partial_y q), \\ T_r \partial_t p &= (\partial_x u - p) + (x-x_j)\,(\partial_x p + \partial_y q), \\ T_r \partial_t q &= (\partial_y u - q) + (y-y_j)\,(\partial_x p + \partial_y q). \end{aligned} \tag{59}$$

Therefore, the extra terms in the last two equations will vanish in the steady state. This system works equally well for constructing a third-order scheme, but it is not considered in this paper because extensions to the advection-diffusion equation would require a new construction, i.e., the advective term also needs to be incorporated into the extra terms. On the other hand, the formulation (54) can be extended to the advection-diffusion equation without any modification.

The construction of a third-order scheme is now straightforward. We simply apply the scheme of Katz and Sankaran to the fully hyperbolic diffusion system (53). No source term discretization is necessary. Also, second derivatives of the source term are not needed. As in the second order schemes, there are two possible constructions for third-order schemes: Scheme I and II.

4.4.2 Third-Order Scheme I

In order to upgrade the second-order scheme to third order, we only need to make two minor modifications. One is to remove the point source term discretization and add the upwind flux for the source-term flux (54). The other is to perform the gradient reconstruction by a quadratic fit (instead of a linear fit). Note that only the coefficients for the gradients are stored for the quadratic fit and the second derivatives are never computed. Consequently, the cost of the quadratic gradient computation is fully comparable to that of the linear gradient computation provided the number of the neighbors involved is comparable.

The energy-estimate for the third-order scheme is the same as the second-order version (36) except that it has the following extra term associated with the consistency constraint on the right hand side:

$$\frac{\nu}{4} \sum_{e\in\{e\}} (\overline{q}\Delta x - \overline{p}\Delta y) \left\{ \Delta(\widetilde{\Delta q}) n_x - \Delta(\widetilde{\Delta p}) n_y \right\} A_{jk}, \tag{60}$$

where $\Delta x = x_k - x_j$, $\Delta y = y_k - y_j$, $\overline{p} = (p_j + p_k)/2$, $\overline{q} = (q_j + q_k)/2$, $\Delta(\widetilde{\Delta q}) = \widetilde{\Delta q}_k - \widetilde{\Delta q}_j$, and $\Delta(\widetilde{\Delta p}) = \widetilde{\Delta p}_k - \widetilde{\Delta p}_j$. It is not clear if this term, which is apparently $O(h^2)$ smaller than others, is positive or negative. Consequently, the third-order scheme is not guaranteed to be energy-stable. The construction of an energy-stable third-order scheme is a subject for future work.

To confirm the third-order accuracy on a regular grid, we substitute smooth functions into the scheme and expand to get

$$\frac{du_j}{dt} = \nu(\partial_x p + \partial_y q) - \frac{\nu h^2}{12}\left[\partial_{xx}(\partial_x p + \partial_y q) + \partial_{xy}(\partial_x p + \partial_y q) + \partial_{yy}(\partial_x p + \partial_y q)\right] + O(h^3), \tag{61}$$

$$\frac{dp_j}{dt} = \frac{1}{T_r}(\partial_x u - p) + \frac{h^2}{12T_r}\left[(\partial_{xx} + \partial_{xy} + \partial_{yy})(p - \partial_x u) - (\partial_x + 2\partial_y)(\partial_x q - \partial_y p)\right] + O(h^3), \tag{62}$$

$$\frac{dq_j}{dt} = \frac{1}{T_r}(\partial_y u - q) + \frac{h^2}{12T_r}\left[(\partial_{xx} + \partial_{xy} + \partial_{yy})(q - \partial_y u) - (\partial_y + 2\partial_x)(\partial_x q - \partial_y p)\right] + O(h^3). \tag{63}$$

Observe that the extra terms introduced in the fully hyperbolic formulation have generated terms proportional to $\partial_x q - \partial_y p$ in the last two equations, which vanish for exact steady solutions. Assuming

that the smooth functions satisfy the steady equation, we therefore find that all second-order error terms vanish, thus giving

$$\tau_u = O(h^3), \tag{64}$$
$$\tau_p = O(h^3), \tag{65}$$
$$\tau_q = O(h^3). \tag{66}$$

The truncation error is, therefore, $O(h^3)$ for all equations. The scheme is truly third-order accurate. We emphasize that this scheme does not require computations of second derivatives.

4.4.3 Third-Order Scheme II

As described in Section 4.3.2 for the second-order scheme, we can replace the least-squares solution gradients in Scheme I by the gradient variables (p_j, q_j). The resulting scheme is still third-order accurate. To see this, we expand the scheme on a regular triangular grid as before to get

$$\begin{aligned}
\frac{du_j}{dt} &= \nu(\partial_x p + \partial_y q) \\
&- \frac{\nu h}{6L_r}\left[(\sqrt{2}+\sqrt{5})\partial_x(p-\partial_x u) + \sqrt{2}\partial_y(p-\partial_x u) + \sqrt{2}\partial_x(q-\partial_y u) + (\sqrt{2}+\sqrt{5})\partial_y(q-\partial_y u)\right] \\
&- \frac{\nu h^2}{12}\left[\partial_{xx}(\partial_x p + \partial_y q) + \partial_{xy}(\partial_x p + \partial_y q) + \partial_{yy}(\partial_x p + \partial_y q)\right] + O(h^3), \\
\frac{dp_j}{dt} &= \frac{1}{T_r}(\partial_x u - p) - \frac{h^2}{6T_r}\left[(\partial_{xx}+\partial_{xy})(q-\partial_y u) + \partial_{xx}(p-\partial_x u) + \partial_y(\partial_x q - \partial_y p)\right] + O(h^3), \\
\frac{dq_j}{dt} &= \frac{1}{T_r}(\partial_y u - q) - \frac{h^2}{6T_r}\left[(\partial_{xy}+\partial_{yy})(p-\partial_x u) + \partial_{yy}(q-\partial_y u) - \partial_x(\partial_x q - \partial_y p)\right] + O(h^3).
\end{aligned} \tag{67}$$

It is clear as all the leading error terms vanish that Scheme II is truly third-order accurate. As can be expected from the existence of the first-order error term, this scheme is stable with the forward Euler time integration. Again, we emphasize that this scheme does not require computations of second derivatives, and moreover it is more economical than Scheme I because gradient computations are not needed for the solution u.

5 Fourier Stability Analysis

In this section, we analyze the stability of the developed schemes by the Fourier analysis on a regular triangular grid. As we have done in Section 4.2 in determining the length scale, we insert a Fourier mode into each spatial discretization and derive the corresponding amplification matrix, $\mathbf{M}$. The eigenvalues of $\mathbf{M}$ are denoted by λ_k where $k = 1, 2, 3$, which are relevant to the stability condition. In what follows, we seek the maximum CFL number for the first, second, and third order schemes, with two time-integration schemes: the forward Euler scheme and a two-stage TVD Runge-Kutta scheme.

5.1 Forward-Euler Time Integration

The stability condition for the forward-Euler time integration is given by

$$|1 + \Delta t \lambda_k| \leq 1, \quad k = 1, 2, 3. \tag{68}$$

We find the maximum CFL number by numerically solving the above inequalities for CFL over a range of frequencies, $(\beta_x, \beta_y) \in [-\pi, \pi] \times [-\pi, \pi]$ where the frequencies are sampled over $N = 500$ intervals in each direction. The results are shown in Figure 2(a) and Table 1. The maximum CFL number for Scheme I is 1.0677 for second order and 1.0743 for third order at $h = 1/8$, but it continues to decreases as h gets smaller ($h = 1/2^n, n = 3, 4, 5, \ldots, 26$) as shown in Figure 2(a) . It is essentially unstable as expected. On the other hand, for Scheme II, the maximum CFL number converges to the limiting value 0.7313 for both second order and third order as $h \to 1/2^{26}$. Therefore, the forward-Euler time integration can be employed to drive the solution to the steady state for Scheme II under the restriction CFL ≤ 0.7313. For the first-order scheme, the maximum CFL number is insensitive to h: 1.3032 for nearly all values of h considered.

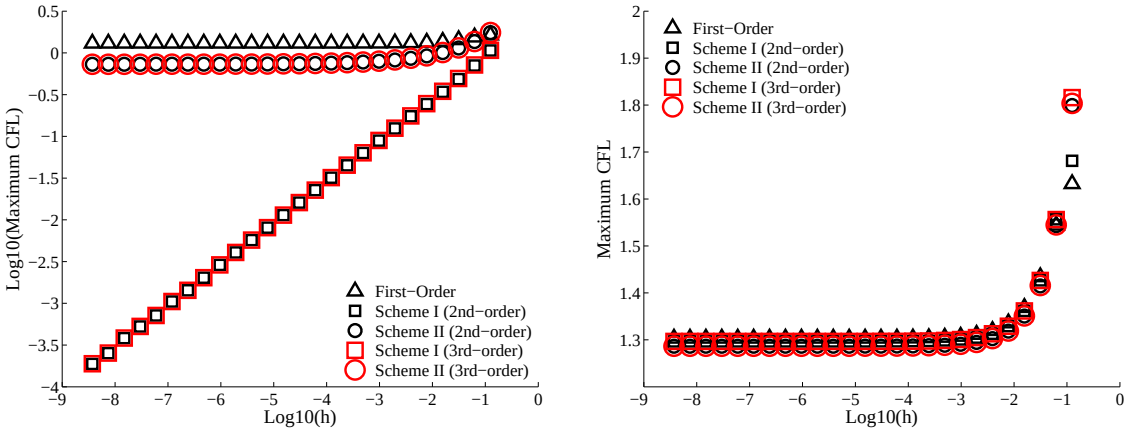

(a) Forward Euler Time Integration

(b) TVD Runge-Kutta Time Integration

Figure 2: Maximum CFL number for $h = 1/2^i,\ i = 3, 4, 5, \ldots, 26$.

	First-Order	Second-Order		Third-Order	
		Scheme I	Scheme II	Scheme I	Scheme II
Forward Euler	1.3032	Unstable	0.7313	Unstable	0.7313
Two-Stage TVD Runge-Kutta	1.3032	1.2967	1.2865	1.2967	1.2865

Table 1: Asymptotic Maximum CFL number ($h = 1/2^{26}$) for the first and second order schemes.

5.2 Two-Stage Runge-Kutta Time Integration

Stable time integration for Scheme I is possible with the two-stage TVD Runge-Kutta time integration [22]. The stability condition is

$$\left|1 + \Delta t\lambda_k + \frac{1}{2}(\Delta t\lambda_k)^2\right| \leq 1, \quad k = 1, 2, 3. \tag{69}$$

For each scheme, we numerically compute the maximum CFL number that satisfies the stability condition as described in the previous section. The results are shown Figure 2(b) and in Table 1. All schemes are conditionally stable with the two-stage TVD Runge-Kutta time integration for practically large CFL numbers around 1.3.

6 Results

We consider a steady diffusion problem in a unit square with the exact solution given by

$$u(x, y) = \frac{\sinh(\pi x)\sin(\pi y) + \sinh(\pi y)\sin(\pi x)}{\sinh(\pi)}. \tag{70}$$

Numerical results are presented for regular and irregular triangular grids with 9×9, 17×17, 33×33, 65×65, 129×129, and 257×257 nodes. The coarsest grids are shown in Figures 3(a) and 3(b). The first, second, and third order upwind schemes for the hyperbolic diffusion systems are compared with the Galerkin scheme directly applied to the diffusion equation (1). We compute the numerical solution by marching in time with the two-stage TVD Runge-Kutta scheme at CFL= 1.28 for second and third order schemes, and by the forward Euler scheme at CFL=1.28 for the first order scheme, at CFL=0.73 for second and third order versions of Scheme II, and at CFL= 0.99 for the Galerkin scheme. The steady state is taken to be reached when the residuals drop below 10^{-15} in the L_1 norm. The initial solution is set up by the exact solution with random perturbation. The Dirichlet boundary condition is applied everywhere on the boundary. The quadratic fit is performed with the nearest neighbors on the regular grids (with stencil extensions for the boundary nodes). For the irregular grids, to avoid possible

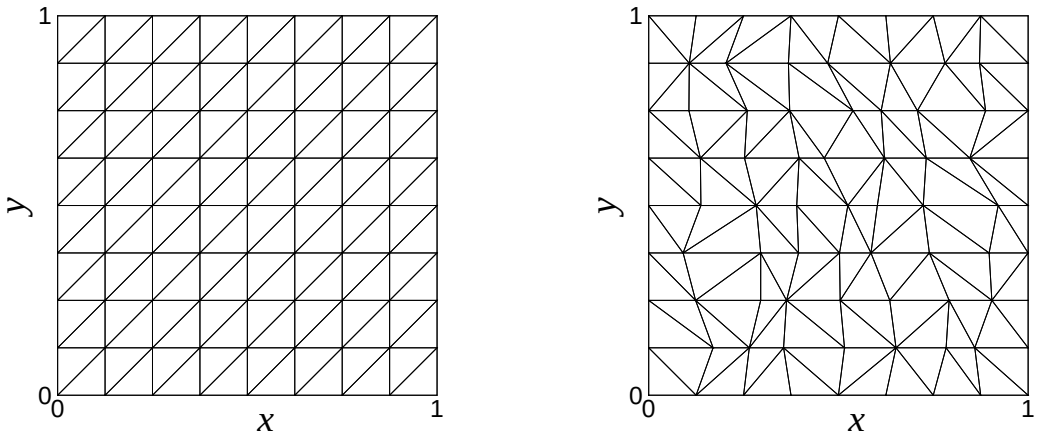

(a) Regular grid

(b) Irregular grid

Figure 3: 9×9 *regular and irregular grids. The irregular grid is generated from the regular grid by random diagonal swapping and nodal perturbation.*

ill-conditioning, we increase the number of neighbors up to 10 by adding neighbors of the neighbors. It should be possible to make the third-order scheme nearly as compact as the second-order scheme by a more sophisticated selection of neighbors. Note that the number of neighbors is typically more than enough in three-dimensional tetrahedral grids to which the edge-based third-order scheme is applicable. In both linear and quadratic fits, the unweighted least-squares method is employed to generate the coefficients, $\mathbf{c}_{jk} = (c^x_{jk}, c^y_{jk})$; the gradients are computed in the form

$$(\nabla u)_j = \sum_{k \in \{k_j\}} \mathbf{c}_{jk}(u_k - u_j). \tag{71}$$

The costs of the linear and quadratic fits are thus comparable on regular grids, but differ on irregular grids by the number of extra neighbors added for the quadratic fit. In the quadratic fit, second derivatives can be computed, but we do not compute them nor store the least-squares coefficients for them because second derivatives are not needed in the third-order scheme.

Error convergence results for the regular grids are shown in Figure 4. The results confirm the design order of accuracy in all variables for all schemes: first, second, and third order accuracy in u and p for first, second, and third order schemes, respectively. Results for q are very similar to those for p, and therefore not shown. In all results, we observe that Scheme II gives more accurate solutions and gradients than Scheme I (compare red and blue lines). Also, we see for second-order accuracy that Scheme I is less accurate than the Galerkin scheme while Scheme II is equally accurate as the Galerkin scheme. For the Galerkin scheme, the gradients are computed by the unweighted linear least-squares method. For these regular triangular grids, the least-squares gradients are second-order accurate at the interior nodes. However, we observe that Scheme I and Scheme II produce more accurate gradients than the linear least-squares gradients even in the second-order case.

Results in Figure 5 confirm the design accuracy of the developed schemes for the irregular grids. We observe again that Scheme II produces consistently more accurate solutions than Scheme I, and the second-order version of Scheme II is comparably accurate with the Galerkin scheme. For the accuracy in the gradients, Scheme I and II produce significantly more accurate gradients than the least-squares gradients computed from the solution of the Galerkin scheme. On the finest grid, the third-order schemes produce nearly three orders of magnitude more accurate gradients than the least-squares gradients. Even the second-order results show almost two orders of magnitude improvements over the least-squares gradients.

It is emphasized that the third-order schemes are only slightly more expensive than the corresponding second-order schemes. The cost per time step measured in the numerical experiment (averages taken over iterations and over all grids in the irregular grid case) is summarized in Table 2. It shows that Scheme I and II require approximately 8% and 6% additional work to upgrade the accuracy from second order to third order. Note also that Scheme II, which does not require gradient computations for the

main variable, is nearly 10% more economical than Scheme I. It is also seen that the per-time-step cost of the Galerkin scheme (implemented in a loop over elements) is lower than any other scheme. However, the Galerkin scheme is the most expensive scheme in terms of the overall cost of obtaining the steady solution as we will see below.

Figures 6(a) and 6(b) show the total time steps (iterations) required to reach the steady state for the regular grids. Figure 6(a) shows, as expected from $O(h^2)$ time step required for traditional diffusion scheme, that the number of iterations increases quadratically (with respect to $1/h$) in the Galerkin scheme whereas it increases linearly in the hyperbolic schemes. Although the cost per iteration is more expensive in the hyperbolic schemes, the $O(1/h)$ acceleration in iterations yields $O(1/h)$ acceleration in the CPU time as shown in Figure 6(b). Note that the acceleration factor grows as the grid gets finer. Furthermore, the convergence acceleration comes with the superior accuracy in the gradients. Comparison among the hyperbolic schemes in Figure 6(b) show that Scheme II converges faster than Scheme I for both second and third order accuracy, and that third-order schemes require only slightly more CPU time than the corresponding second-order schemes. Similar results are obtained for irregular grids, and shown in Figure 7.

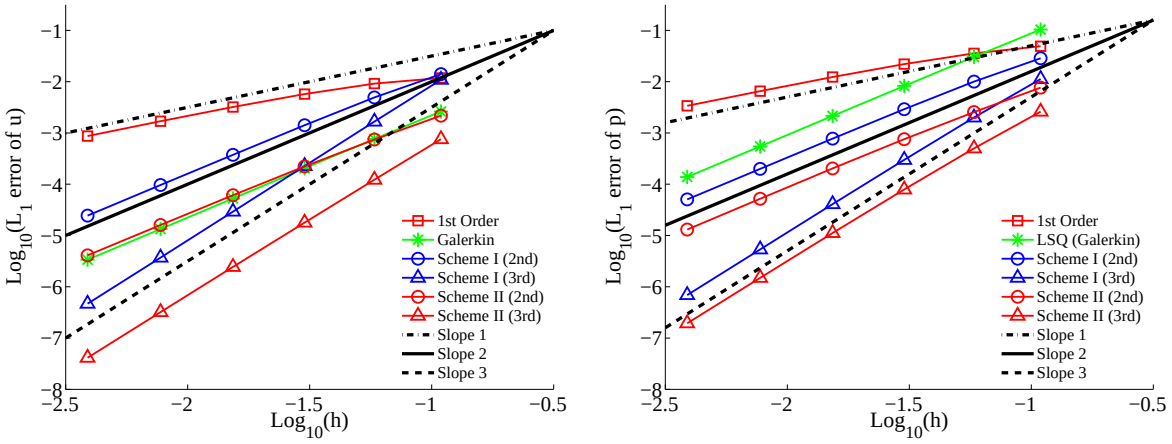

(a) Error in u (b) Error in p

Figure 4: Error convergence results for regular grids. h is the effective mesh spacing defined as the L_1 norm of the square root of the dual volume.

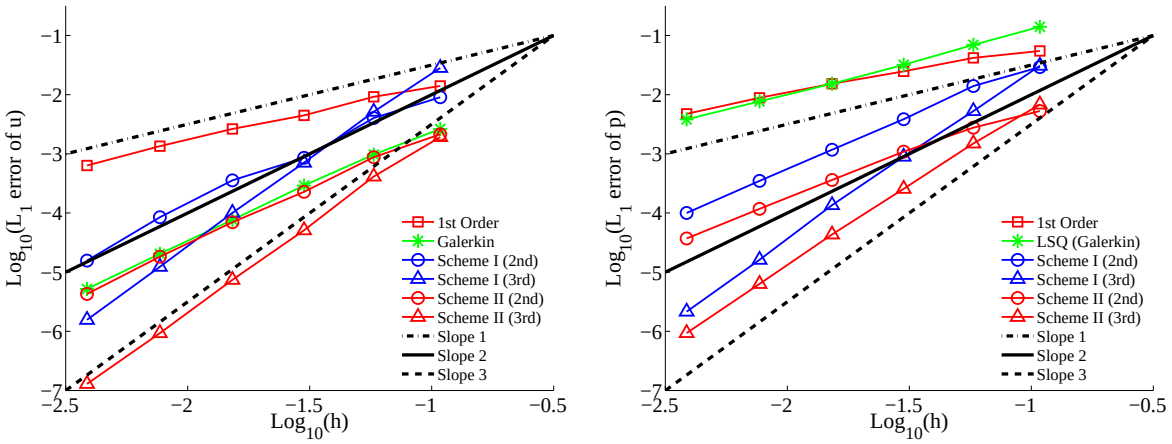

(a) Error in u (b) Error in p

Figure 5: Error convergence results for irregular grids. h is the effective mesh spacing defined as the L_1 norm of the square root of the dual volume.

	Galerkin	First-Order	Second-Order		Third-Order	
			Scheme I	Scheme II	Scheme I	Scheme II
Forward Euler	0.66	1.00		1.26		1.33
Two-Stage TVD RK			2.78	2.53	2.99	2.68

Table 2: Comparison of the cost per time step with respect to the cost of first-order scheme based on the CPU time measured in the irregular grid case.

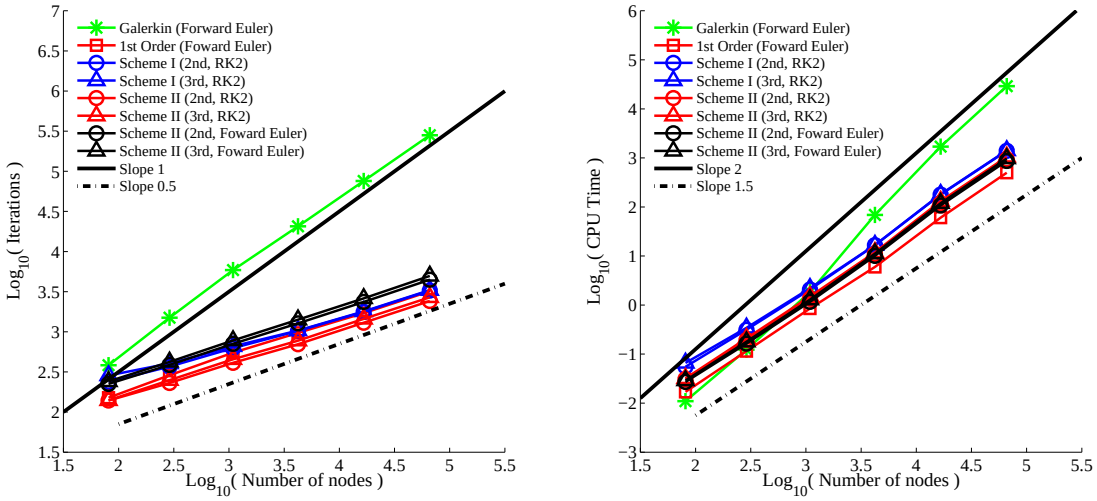

(a) Iteration (b) CPU time

Figure 6: Iteration and CPU time required to reach the steady state for regular grids.

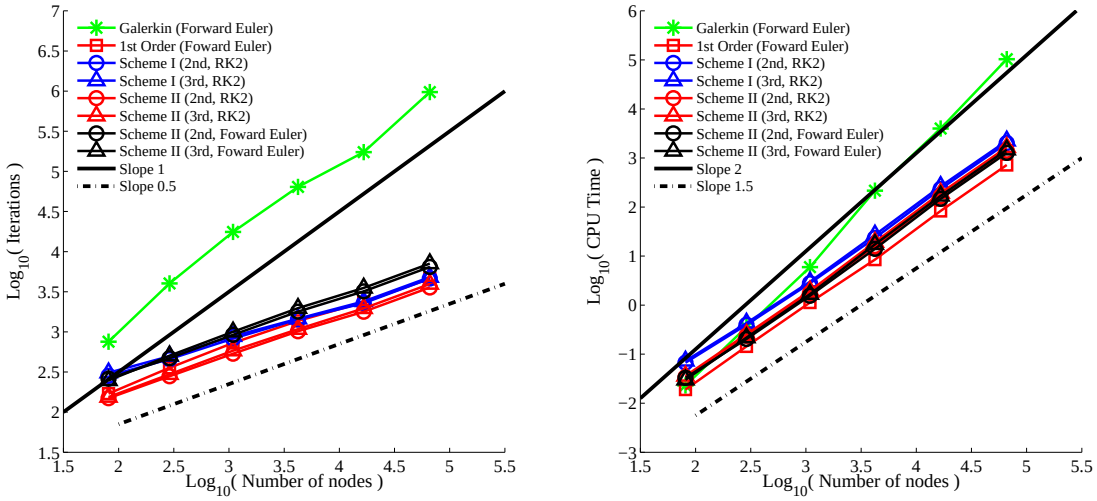

(a) Iteration (b) CPU time

Figure 7: Iteration and CPU time required to reach the steady state for irregular grids.

7 Concluding Remarks

In this paper, we have constructed and analyzed first, second, and third order finite-volume schemes for diffusion on unstructured grids. The energy estimate has been derived for the hyperbolic diffusion system, which is equivalent to the well-known energy estimate of Laplace's equation in the steady state. The first-order scheme has been shown to be energy-stable with the upwind flux, which is readily applicable to the diffusive term in turbulence model equations as well as to the viscous terms in the Navier-Stokes equations [12]. It is emphasized that the developed energy-stable first-order diffusion scheme is applicable to both node-centered and cell-centered finite-volume methods for fully irregular grids of any element type.

Two types of constructions have been considered for second and third order schemes: Scheme I and Scheme II. Scheme I corresponds to a common edge-based finite volume construction for hyperbolic systems. Scheme II employs the gradient variables in the reconstruction for the main variable, resulting in second and third order schemes that are stable with the forward-Euler time integration. In both second and third order accuracy, Scheme II was shown to converge faster and give more accurate solution and gradients than Scheme I. Superior accuracy and efficiency over the Galerkin scheme has been demonstrated by numerical results for both regular and irregular triangular grids. In particular, the developed second- and third-order schemes have been shown to yield second- and third-order accurate gradients, respectively, on irregular grids.

The most striking advantage of the third-order schemes developed here is that third-order accuracy achieved in the gradients nearly at the cost of second-order hyperbolic schemes, which is already more efficient by factor $O(1/h)$ than traditional diffusion schemes. Even in the second-order schemes, the gradients are computed to second order accuracy along with $O(1/h)$ acceleration. As it typically requires third and fourth order schemes to achieve second and third order accuracy in the gradients, the developed second and third order schemes are expected to offer tremendous improvements in efficiency for diffusion problems.

We note that the schemes generated based on the hyperbolic method cannot be time accurate with explicit time integration schemes. Time-accurate computations are possible only with implicit time integration schemes, including space-time methods. The development of time-accurate hyperbolic schemes based on the backward-difference time integration is currently underway, and will be reported elsewhere. We note also that the extension of the hyperbolic method to more complex systems requires a careful study in the construction of a first-order hyperbolic system. As discussed in Ref.[12], a first-order formulation of the compressible Navier-Stokes equations having a simple eigen-structure has not been found yet. To avoid this difficulty, a strategy was proposed in Ref.[12] based on a separate treatment of the inviscid and viscous terms each of which can be independently analyzed and proved to be hyperbolic. The strategy is currently being studied for a model advection-diffusion equation. The details will be reported in a subsequent paper. Note finally that the number of extra variables required in the hyperbolic method can be substantially high for complex systems. For the three-dimensional compressible Navier-Stokes equations, 6 viscous stresses and 3 heat fluxes will be required, at least. It remans to be investigated that the advantages of the hyperbolic method overwhelm any complication arising from a large number of extra variables, or that the hyperbolic method offers a resolution of problems encountered by the current state-of-the-art CFD solvers.

Acknowledgments

This work has been funded by the U.S. Army Research Office under the contract/grant number W911NF-12-1-0154 with Dr. Frederick Ferguson as the program manager. The work was supported partly by the NASA Fundamental Aeronautics Program through NASA Research Announcement Contract NNL12AB00T. Support by Software CRADLE is also greatly acknowledged.

References

[1] W. Johnson and A. Datta. Requirements for next generation comprehensive analysis of rotorcraft. In *Proc. of AHS Specialist Conference on Aeromechanics*. San Francisco, CA, January 2008.

[2] Jeffrey A. Housman and Michael F. Barad. Space-time accuracy assessment of CFD simulations for the launch environment. In *29th AIAA Applied Aerodynamics Conference*, AIAA-2011-3650, 2011.

[3] Graham V. Candler, Dimitri J. Mavriplis, and Loretta Trevino. Current status and future prospects for the numerical simulation of hypersonic flows. AIAA Paper 2009-153, 2009.

[4] P. A. Gnoffo. Multi-dimensional, inviscid flux reconstruction for simulation of hypersonic heating on tetrahedral grids. AIAA Paper 2009-599, 2009.

[5] K. Kitamura, E. Shima, Y. Nakamura, and P. L. Roe. Evaluation of euler fluxes for hypersonic heating computations. *AIAA J.*, 48(4):763–776, 2010.

[6] P. A. Gnoffo. Updates to multi-dimensional flux reconstruction for hypersonic simulations on tetrahedral grids. AIAA Paper 2010-1271, 2010.

[7] K. Kitamura and E. Shima. Improvements of simple low-dissipation ausm against shock instabilities in consideration of interfacial speed of sound. In *Proceedings of ECCOMAS CFD 2010*, Paper No.1283, Lisbon, Portugal, 2010.

[8] H. Nishikawa, B. Diskin, and J. L. Thomas. Critical study of agglomerated multigrid methods for diffusion. *AIAA J.*, 48(4):839–847, April 2010.

[9] H. Nishikawa. Beyond interface gradient: A general principle for constructing diffusion schemes. In *40th AIAA Fluid Dynamics Conference and Exhibit*, AIAA Paper 2010-5093, Chicago, 2010.

[10] H. Nishikawa. A first-order system approach for diffusion equation. I: Second-order residual-distribution schemes. *J. Comput. Phys.*, 227:315–352, 2007.

[11] H. Nishikawa. A first-order system approach for diffusion equation. II: Unification of advection and diffusion. *J. Comput. Phys.*, 229:3989–4016, 2010.

[12] H. Nishikawa. New-generation hyperbolic Navier-Stokes schemes: $O(1/h)$ speed-up and accurate viscous/heat fluxes. In *20th AIAA Computational Fluid Dynamics Conference*, AIAA Paper 2011-3043, Hawaii, 2011.

[13] A. Katz and V. Sankaran. Mesh quality effects on the accuracy of CFD solutions on unstructured meshes. *J. Comput. Phys.*, 230:7670–7686, 2011.

[14] C. Cattaneo. A form of heat-conduction equations which eliminates the paradox of instantaneous propagation. *Ct. R. Acad. Sci., Paris*, 247:431–433, 1958.

[15] A. Jameson. Time dependent calculations using multigrid, with applications to unsteady flows past airfoils and wings. AIAA Paper 91-1596, 1991.

[16] N. D. Melson, M. D. Sanetrik, and E. L. Atkins. Time accurate Navier-Stokes calculations with multigrid acceleration. In *6th Copper Mountain Conference on Multigrid Methods*, (NASA CP 3224), Copper Mountain, 1993.

[17] B. Diskin and J. L. Thomas. Accuracy analysis for mixed-element finite-volume discretization schemes. *NIA Report No. 2007-08*, 2007.

[18] A. Katz and V. Sankaran. An efficient correction method to obtain a formally third-order accurate flow solver for node-centered unstructured grids. *J. Sci.Comput.*, 51:375–393, 2012.

[19] B. Diskin and J. L. Thomas. Effects of mesh regularity on accuracy of finite-volume schemes. In *50th AIAA Aerospace Sciences Meeting*, AIAA Paper 2012-0609, Nashville, Tennessee, 2012.

[20] H. Nishikawa. Divergence formulation of source term. *J. Comput. Phys.*, 231:6393–6400, 2012.

[21] B. B. Pincock and A. Katz. High-order flux correction for viscous flows on arbitrary unstructured grids. In *21st AIAA Computational Fluid Dynamics Conference*, AIAA Paper 2011-2566, San Diego, California, June 2013.

[22] S. Gottlieb and C.-W. Shu. Total variation diminishing Runge-Kutta schemes. *Mathematics of Computation*, 67(221):73–85, 1998.